Applied Chemical Engineering (2026) Volume 9 Issue 2 ISSN: 2578-2010 (O)
doi: 10.59429/ace.v9i2.6010

RESEARCH ARTICLE

Thermochemical Characterization and Process-Oriented Evaluation of Clayey Materials from M'sila (Algeria) for Sustainable Composite Engineering Applications

Deghfel Nadir[1], Laib Nouri[2], Benyahia Azzedine[1,*], Melouki Azzedine[2], Larkat Karima[1], Djehiche Mokhtar[2]

[1] *City, Environment, Hydraulics and Sustainable Development Laboratory, Sciences faculty, Mohamed Boudiaf University M'sila, 28000, Algeria*

[2] *Inorganics Materials Laboratory, Sciences faculty, Mohamed Boudiaf University M'sila, 28000, Algeria*

***Corresponding author:** Benyahia Azzedine, azzedine.benyahia@univ-msila.dz

ABSTRACT

The growing demand for sustainable and low-carbon construction materials has stimulated increasing interest in the valorization of natural clayey resources and plant-based reinforcements for eco-friendly composite applications. However, the thermochemical behavior, mineralogical complexity, and engineering performance of natural clayey materials from semi-arid regions remain insufficiently understood. In this study, three representative clayey materials (Red, Green, and Yellow) collected from the Soubella region (M'sila, Algeria) were investigated to evaluate their suitability for sustainable clay-based composite engineering applications.

A multi-analytical methodology combining X-ray diffraction (XRD), X-ray fluorescence (XRF), Fourier transform infrared spectroscopy (FTIR), thermogravimetric and derivative thermogravimetric analyses (TGA/DTG), scanning electron microscopy (SEM), and energy-dispersive X-ray spectroscopy (EDX) was employed to characterize the mineralogical composition, chemical reactivity, thermal transformations, granulometric distribution, and microstructural evolution of the investigated materials. The influence of untreated Cynodon dactylon fibre reinforcement on the physicochemical and mechanical behavior of clay-based composites was also evaluated.

Granulometric and physicochemical analyses revealed that the Red and Green clayey materials are dominated by fine clay–silt fractions, whereas the Yellow material exhibits a comparatively higher carbonate-rich sandy composition. Mineralogical characterization identified quartz- and illite-rich phases in the Red and Green materials, while the Yellow material showed a higher calcite concentration. Thermogravimetric analyses highlighted distinct thermal transformation pathways associated with dehydration, dehydroxylation, and carbonate decomposition reactions. The obtained thermal profiles confirmed the thermal stability and activation potential of the investigated materials at elevated processing temperatures. Mechanical investigations demonstrated that natural fibre incorporation significantly improved the compressive and flexural performances of the clay-based composites by enhancing matrix cohesion and fibre-matrix interfacial interactions. In particular, the Yellow clay composite reinforced with untreated Cynodon dactylon fibres exhibited a notable increase in flexural strength compared with the unreinforced systems. Overall, the results demonstrate that mineralogical composition, thermal behavior, and natural fibre reinforcement strongly influence the engineering performance of clay-based composites. The investigated materials therefore constitute promising low-carbon resources for the development of eco-friendly composite materials and sustainable construction systems adapted to semi-arid environments.

Keywords: thermochemical behavior; clay composites; thermal transformation; process engineering; natural fiber reinforcement; sustainable materials.

ARTICLE INFO

Received: 20 April 2026
Accepted: 15 May 2026
Available online: 28 May 2026

1. Introduction

With the rise of industrialization, the world is facing significant challenges related to increasing greenhouse gas emissions from both natural and anthropogenic sources, which contribute substantially to global warming. Among the major contributors to these emissions are the construction sector and industrial activities, both of which require high energy consumption [1–3]. In response to population growth and the increasing demand for construction materials, the development of natural and eco-friendly alternatives has become a critical priority. In this context, clay-based systems have attracted increasing attention not only as sustainable construction materials but also as reactive aluminosilicate resources capable of undergoing physicochemical and thermochemical transformations relevant to low-carbon engineering applications.

In Algeria, earthen constructions, particularly in arid rural areas and southern regions, have endured for decades. This architectural heritage, combined with growing environmental concerns, has renewed interest in clay-based materials for sustainable construction. Clayey materials are considered promising alternatives to cement and conventional aggregates, with the potential to reduce the environmental footprint of buildings [4–7]. These materials offer several advantages, including wide availability, low cost, environmental compatibility, good thermal insulation properties, relatively low shrinkage, and satisfactory mechanical performance [8–10].

Recent investigations dealing with the behavior of soft soils under dynamic and structural loading conditions have further highlighted the importance of detailed physicochemical characterization of fine-grained geomaterials. For example, studies on tunnel complexes constructed in soft soils subjected to seismic vibrations demonstrated that mineralogical composition, granulometric distribution, and soil fabric strongly influence deformation mechanisms, stress transfer, and long-term engineering stability [11,12]. These findings emphasize the necessity of integrating geotechnical, mineralogical, and microstructural analyses when evaluating clayey materials for sustainable engineering applications. Beyond their physical properties, clayey systems also exhibit significant chemical reactivity associated with the transformation of aluminosilicate and carbonate phases during thermal or alkaline activation. Such transformations, including dehydroxylation, decarbonation, and amorphization phenomena, strongly influence the pozzolanic activity and engineering performance of clay-based composites. Mineralogical studies, such as that of Naghizadeh-Ardebili et al. [13] on the Kashafrud Formation in Iran, have provided valuable insights into the compositional variability of clayey materials and their potential applications. These studies emphasize the importance of detailed geochemical and mineralogical characterization to optimize the use of such natural resources. However, recent advances in sustainable process engineering indicate that the valorization of clayey materials should also consider the kinetics of thermal transformations and the efficiency of chemical activation processes. In particular, thermally activated clay minerals can generate reactive amorphous phases capable of participating in pozzolanic reactions and secondary binding mechanisms.

Several recent studies employing FTIR, XRD, SEM, TGA/DTG, and microstructural analyses have demonstrated the importance of mineralogical characterization in understanding the durability, reactivity, and physicochemical evolution of sustainable cementitious and aluminosilicate systems. Investigations on sulfate-resistant cementitious composites and seawater coral-aggregate concretes showed that mineralogical transformations, hydration products, and carbonate reactions strongly affect durability and mechanical performance under aggressive environmental conditions [14–16]. Likewise, studies dealing with carbonation resistance, steel slag mortars exposed to sulfate attack, and thermochemical evolution of sulfoaluminate systems highlighted the critical role of phase transformations and microstructural modifications in controlling the long-term stability and engineering behavior of eco-friendly materials [17–20]. Additional studies focusing on the mineralogical evolution of cementitious systems using FTIR, XRD, and thermogravimetric analyses demonstrated that hydration, carbonation, and thermal decomposition reactions govern the development of reactive amorphous phases and influence mechanical performance [21,22]. These studies provide valuable

methodological references for interpreting the FTIR, XRD, SEM, and TGA/DTG results obtained in the present work. Consequently, numerous researchers have focused on the development of clayey matrices reinforced with natural fibers to produce sustainable construction composites. Clayey materials therefore represent not only an important economic resource in construction, ceramics, and environmental applications, but also a versatile class of reactive mineral systems with potential applications in catalysis, adsorption, and chemically engineered composite materials [23–25]. Despite the abundance of clayey resources in Algeria, few studies have specifically addressed the geological characteristics, thermal behavior, and chemical reactivity of materials from the M'sila region. To the best of our knowledge, detailed investigations of these materials remain limited, which justifies the relevance of the present work. Kouadri et al. [26] reinforced red clayey materials with palm fibers treated with a 4% NaOH solution and reported a significant improvement in mechanical properties, highlighting the role of alkaline surface activation in enhancing matrix–fiber interactions. Elhamdouni et al. [27] developed a composite material combining clayey soil with Alfa fibers and showed that its high contents of SiO_2 (45.79%), Al_2O_3 (15.68%), and Fe_2O_3 (12.83%) contributed to enhanced mechanical performance and potentially increased aluminosilicate reactivity. Deghfel et al. [28] studied three types of clayey materials from the M'sila region and reported that the Yellow material is mainly composed of quartz and illite, reaching up to 47%. The Green material contains calcite, quartz, illite, and kaolinite, whereas the Red material consists of a mixture of calcite, quartz, and illite. The presence of kaolinite and carbonate phases is particularly important because these minerals undergo thermally induced dehydroxylation and decarbonation reactions, which directly affect the formation of reactive phases during thermal activation. Mouissa et al. [29] developed clay-based composites reinforced with sawdust treated using permanganate and soda solutions for rural construction applications.

Their chemical analysis showed that silica and alumina are the dominant oxides, with contents of 35.21% and 13.62%, respectively, indicating an aluminosilicate matrix rich in calcite ($CaCO_3$). Fung et al. [30] investigated the mechanical strength and drying behavior of earthen materials derived from different soil types used in traditional construction. Their results showed that compressive strength increases as moisture content decreases. However, despite the renewed interest in earthen construction and the recognized importance of these resources, the mineralogical, thermal, and reactive properties of clayey materials from the M'sila basin remain insufficiently documented. This lack of detailed physicochemical and thermochemical characterization limits the understanding of their transformation pathways, activation efficiency, and suitability for sustainable process-oriented construction applications.

The present study aims to develop sustainable clay-based composite materials using three natural clayey materials (Red, Green, and Yellow) reinforced with untreated *Cynodon dactylon* fibres for potential application in eco-friendly construction bricks. Particular attention is devoted to evaluating the influence of mineralogical composition, granulometric characteristics, and fibre reinforcement on the physicochemical, thermochemical, microstructural, and mechanical behavior of the developed composites. The objective is to assess the suitability of these locally available natural resources for the production of low-carbon and sustainable construction materials with improved engineering performance.

2. Materials and methods

2.1. Reinforcement fibre: Cynodon dactylon

The natural fiber used as reinforcement in this study was *Cynodon dactylon*. Representative photographs of the raw fibres and SEM micrographs illustrating their surface morphology are presented in **Figure 1**. Its lignocellulosic composition, determined by the Kalson method, consisted of 30.88% cellulose, 23.84% hemicellulose, and 18.64% lignin, representing a total structural organic content of approximately 73.36%. The fibres exhibited a rough and irregular surface morphology characterized by longitudinal fibrillar structures, which are favorable for mechanical interlocking and fibre-matrix adhesion within clay-based composites. The

low apparent density (0.9 g·cm^{-3}), measured by air-displacement pycnometry, indicates a porous and lightweight morphology typical of non-woody lignocellulosic fibers, consistent with recent reports on natural fiber composition and structure [31]. Such fibers are widely recognized for their cellulose-rich structure and hierarchical organization, which govern their mechanical performance and suitability as reinforcements in composite materials. These characteristics make *Cynodon dactylon* fibers promising bio-based reinforcements for clay-, lime-, and cement-based matrices, due to their ability to enhance mechanical properties while contributing to the development of sustainable and environmentally friendly composite materials.

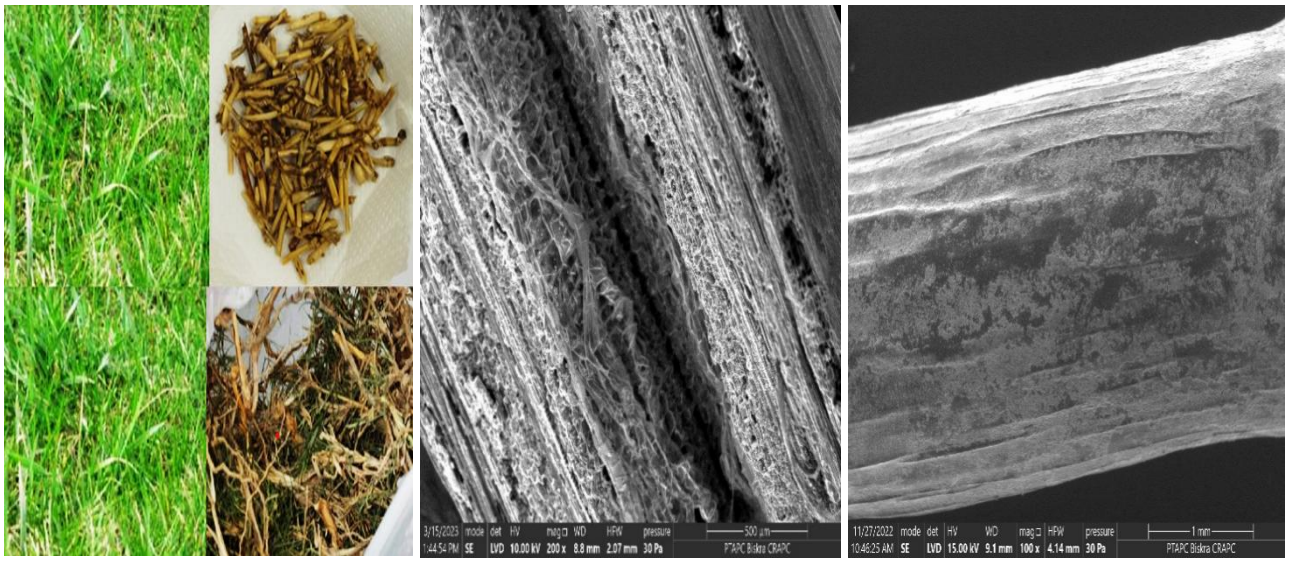

Figure 1. Morphological characterization of raw Cynodon dactylon fibres using photographic and SEM observations

2.2. Sampling Site and Collection Procedure

Three clayey material samples were collected from the Soubella region, located approximately 60 km northeast of the city of M'sila, Algeria (**Figure 2**). This area is characterized by sedimentary formations composed of fine-grained materials, making it particularly suitable for the present investigation. Sampling was carried out manually at a depth of 40 cm to minimize surface contamination due to weathering and anthropogenic activities, ensuring that the collected materials are representative of the natural subsurface composition.

To ensure representativeness, multiple subsamples were collected and combined into composite samples. After collection, the samples were air-dried under ambient conditions for 14 days to stabilize their moisture content. The dried materials were then crushed using a mortar and pestle, followed by mechanical grinding to obtain fine powders. The powders were subsequently sieved using a RETSCH sieve shaker equipped with a 50 µm mesh in order to isolate the fine mineral fraction for physicochemical, mineralogical, and spectroscopic analyses. The use of the 50 µm fraction allows enrichment of clay-associated minerals and improves the reliability of XRD and FTIR characterization by reducing the influence of coarse silicate particles [32-34]. The use of a particle-size threshold below 50 µm is commonly adopted in soil and clay mineral characterization to isolate the fine fraction enriched in clay-associated phyllosilicate minerals [35-37]. Fine particle fractions are known to govern most of the physicochemical and reactive properties of clayey materials due to their high specific surface area and elevated phyllosilicate content [35,37]. The enrichment of this fine fraction enhances the reliability of mineralogical and spectroscopic analyses by reducing the influence of coarse quartz-rich particles and improving the detection of clay-related phases such as illite and kaolinite [37].

The selected sampling depth (40 cm) further ensures reduced influence of surface alterations and better represents the relatively unweathered subsurface horizon characteristic of the geological context of the M'sila region [38,39].

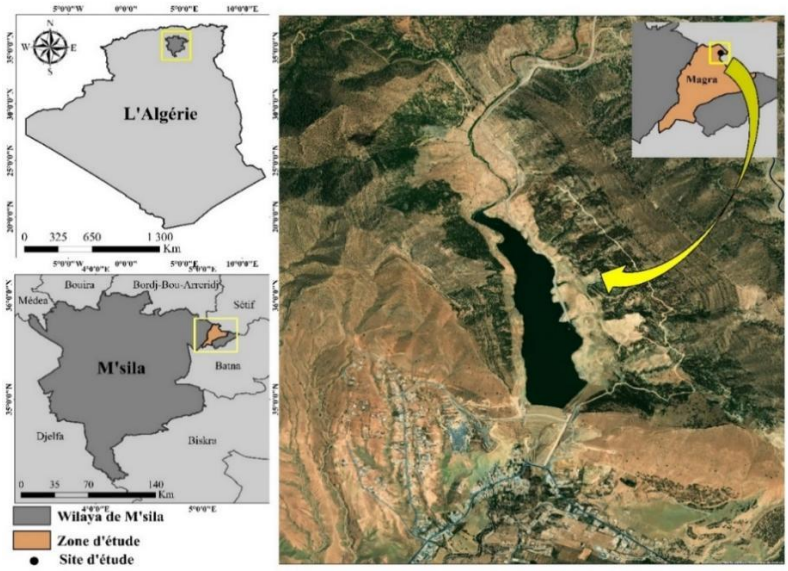

Figure 2. Location of the sampling site

Representative photographs of the Red, Green, and Yellow clayey materials collected from the Soubella region are shown in **Figure 3**. The visible differences in color and texture suggest variations in mineralogical composition and particle-size distribution, which were further investigated through physicochemical and mineralogical analyses.

Figure 3. Representative photographs of clayey materials (red, green, and yellow) collected from the Soubella region

2.3. Preparation of Composite Materials

The composite materials were prepared using locally sourced clay collected from the Soubla region (M'Sila, Algeria). For composite preparation, the raw clay materials were sieved to a particle size below 100 µm and subsequently dried at 65 ± 2 °C for 24 h to eliminate residual moisture. Unlike the <50 µm fraction used for mineralogical characterization, the 100 µm fraction was selected to preserve a broader particle-size distribution more representative of clay-based construction materials. This granulometric choice is expected to improve particle packing, workability, and fibre–matrix interaction during composite processing. Particle size is also known to strongly influence water demand, compaction behavior, porosity, and the mechanical performance of clay-based composites. Portland cement CEM I 42.5N-SR3 supplied by Lafarge M'Sila

(Algeria) was used as the primary hydraulic binder, while quicklime produced in Saida (Algeria) and silica fume provided by Master Builders Solutions Algeria were incorporated to enhance stabilization through cementitious and pozzolanic reactions. Potable water complying with the NF P 18-404 standard was used for all formulations at a controlled temperature of 20±2°C. The dry constituents were first premixed mechanically for 2 min using a laboratory mixer to ensure initial homogenization of the mineral components, followed by the gradual addition of water and controlled manual mixing for approximately 5 min until a visually homogeneous paste was obtained. Manual homogenization was performed to minimize fibre agglomeration and improve fibre dispersion within the clay matrix. The resulting mixtures were cast into prismatic molds (4 × 4 × 16 cm^3), air-dried for 72 h, demolded, and subsequently cured for 7 days at 65°C in sealed plastic bags. Based on the optimization study, the final formulation consisted of clay mixed with 12 wt.% cement, 9 wt.% lime, and 5 wt.% silica fumes. Untreated *Cynodon dactylon* fibres were incorporated at a constant content of 3 wt.%. The selected fibre content was determined based on preliminary optimization tests and previous studies indicating that fibre additions between 2 and 4 wt.% generally provide improved crack resistance and mechanical reinforcement while avoiding excessive porosity, fibre clustering, and loss of workability. A sequential mixing procedure was employed, involving the pre-mixing of the binders, addition of water, incorporation of fiber, and final homogenization to ensure uniform dispersion within the matrix. **Table 1** summarizes the abbreviations and designations of the prepared composites used in this study.

The curing temperature of 65 °C was selected to accelerate pozzolanic and hydration reactions while limiting excessive thermal degradation of the natural fibres.

Representative photographs of the prepared composite specimens after molding, curing, and demolding are presented in **Figure 4**. The images illustrate the surface appearance, dimensional homogeneity, and fibre distribution within the clay-based matrices.

Table 1. Designation and composition of the prepared composites

Sample code	Composite
AJ	Yellow clay
AJFNT	Yellow clay reinforced with untreated *Cynodon dactylon* fibers.
AR	Red clay
ARFNT	Red clay reinforced with untreated *Cynodon dactylon* fibers.
AV	Green clay
AVFNT	Green clay reinforced with untreated *Cynodon dactylon* fibers.

Figure 4. Photographs of prepared clay-based composite specimens reinforced with *Cynodon dactylon* fibres.

2.4. Physical and Chemical Characterization

2.4.1. pH Measurement

The pH was measured to evaluate the acidity or alkalinity of the clayey materials in aqueous suspension, as it directly influences ion exchange processes and mineral stability. A 10 % (w/v) suspension of the material in distilled water was prepared and allowed to equilibrate at 25 °C for 4 h to ensure stabilization of the system. The suspension was then homogenized using a magnetic stirrer prior to pH measurement with a calibrated HANNA digital pH meter. All measurements were performed in triplicate to ensure reproducibility and reliability.

2.4.2. Moisture Content

The moisture content was determined based on the weight loss of a wet sample after drying at 105 ± 5 °C for 24 h. The dry mass (Wdry) was recorded, and the moisture content (MC) was calculated using the Equation. (1):

$$MC(\%) = \frac{(W_{wet} - W_{dry})}{W_{dry}} x\ 100 \quad (1)$$

where W_{wet} is the mass of wet sample (g) and W_{dry} is the mass after oven drying (g).

All measurements were performed in triplicate, and the average values are reported.

2.4.3. Swelling Index (SI)

The swelling index quantifies the volume increase of clay upon water absorption and is relevant for assessing dimensional stability. A 100 mL graduated cylinder was filled with 50 mL of distilled water, and then 0.5 g of clay was added. After 45 min, an additional 0.5 g of clay was introduced. The final volume of the swollen clayey material was recorded after 2 h. The swelling index was calculated using Equation (2):

$$SI(\%) = \frac{W_{swollen} - W_{dry}}{W_{dry}} X\ 100 \quad (2)$$

where, W_{dry}: dry weight of the sample; $W_{swollen}$: weight of the sample after swelling.

Measurements were repeated twice to confirm consistency [40].

2.4.4. Loss on Ignition (LOI)

LOI indicates the content of volatile components such as structural water, organic matter, and carbonates, which affect thermal behavior. Pre-weighed samples were heated to 1000 °C for 1 h in a muffle furnace. The procedure involved placing a pre-weighed sample in the furnace, heating it, and then reweighing the sample after cooling. LOI (%) was calculated based on the difference between the initial and final masses [41], using Equation (3):

$$LOI(\%) = \frac{(P_1 - P_2)}{P_1} X100 \quad (3)$$

The measurements were conducted in triplicate to ensure reproducibility.

2.4.5. X-ray Fluorescence (XRF)

The chemical composition of the clayey material samples was determined by X-ray fluorescence (XRF) spectrometry. The analyses were performed using a Bruker AXS GmbH spectrometer (Karlsruhe, Germany). Measurements were carried out at the Lafarge cement plant laboratory in M'sila, Algeria.

2.5. Geotechnical characterization

2.5.1. Atterberg Limits

The consistency and plasticity of the clayey material samples were evaluated according to the French standard NF P 94-051 [42]. Each geotechnical parameter was measured at least three times, and the reported values correspond to the mean results.

2.5.2. Liquid Limit (LL)

The liquid limit (LL) was determined using the Casagrande cup method. A paste of the clayey material was placed in the brass cup, and a groove was cut along the center using a standard grooving tool. The cup was then repeatedly dropped from a specified height, and the number of blows required to close the groove over a distance of 12.7 mm (½ inch) was recorded. The corresponding water content was taken as the liquid limit.

2.5.3. Plastic Limit (PL)

The plastic limit (PL) was determined using the rolling method. A portion of the clayey material was rolled by hand into threads until they crumbled at a diameter of approximately 3 mm. The corresponding water content at this stage was defined as the plastic limit.

2.5.4. Plasticity Index (PI)

The plasticity index (PI) is a numerical value that defines the range of water content over which a soil exhibits plastic behavior. This index reflects the soil's capacity to undergo deformation while maintaining cohesion without cracking or crumbling. It is calculated as the difference between the liquid limit (LL) and the plastic limit (PL), as shown in Equation (4):

$$PI = \mathrm{LL} - \mathrm{PL} \qquad (4)$$

2.5.5. Particle Size Distribution by Laser Diffraction

Particle size distribution was analyzed using a Mastersizer 3000 laser diffraction analyzer (Malvern Panalytical), operating over a measurement range of 10 nm to 3.5 mm. The procedure followed ISO 13320:2020 for laser diffraction methods, which defines the requirements for optical modeling, sample dispersion, measurement reliability, and data quality. This technique provides high-resolution granulometric profiles, enabling an accurate assessment of the textural characteristics of the clay materials and their influence on associated mechanical properties.

2.6. Structural and Mineralogical Characterization

Structural and mineralogical characterization of the clayey materials was carried out using complementary analytical techniques. Fourier transform infrared (FTIR) spectroscopy was performed to identify the functional groups present in the samples using a Shimadzu FTIR-8300 spectrometer over the spectral range of 400–4000 cm^{-1}. For the analysis, 1 g of clay previously dried at 105 °C was mixed with KBr in a 1:100 ratio before spectral acquisition. The crystalline structure and mineral phases of the powdered samples were investigated by X-ray diffraction (XRD) using a Bruker D8 ADVANCE diffractometer (Karlsruhe, Germany) equipped with Cu-Kα radiation (λ = 1.5418 Å). Quantitative phase analysis was performed using Rietveld refinement implemented in dedicated XRD analysis software. The refinement procedure enabled semi-quantitative estimation of the crystalline mineral phases present in the samples. Particular attention was paid to possible peak overlap effects between carbonate and phyllosilicate minerals.

The thermal behavior of the clayey materials was examined through thermogravimetric analysis (TGA) using a TA-60 WS analyzer (Shimadzu Corp., Kyoto, Japan) under a nitrogen flow of 80 mL/min, with a heating rate of 10 °C/min over a temperature range of 30–1000 °C. In addition, the surface morphology and

particle arrangement of the samples were observed by scanning electron microscopy (SEM) using a JEOL JSM-7001F microscope operated at an accelerating voltage of 15 kV.

The mineralogical interpretation was established through the complementary use of FTIR and XRD techniques. Particular attention was paid to possible discrepancies between the two methods, especially regarding clay mineral quantification. FTIR analysis may underestimate certain clay phases because of band overlap, weak absorption intensity, or masking effects caused by dominant silicate vibrations, whereas XRD provides a more direct identification and semi-quantitative estimation of crystalline mineral phases. Therefore, the interpretation of clay mineral abundance was based on the combined assessment of both techniques rather than on a single analytical method.

2.7. Mechanical Testing

2.7.1. Flexural Test

The mechanical properties of the specimens were evaluated using an Automax Multitest universal testing machine (Italy) with a maximum load capacity of 100 kN. In accordance with the NF EN 196-1 standard, three-point bending tests were performed on prismatic specimens measuring 4 × 4 × 16 cm³ at a constant loading rate of 0.5 mm/min. The flexural strength, σ_f (MPa), was calculated using Equation (5):

$$\sigma_f = \frac{3FL}{2bh^2} \quad (5)$$

where F is the maximum applied load (N), L is the span length between supports (mm), b and h are the width and height of the specimen (mm), respectively.

2.7.2. Compressive Test

The compressive behavior of the materials was characterized using an Automax 5 automatic compression testing machine (Italy) with a loading capacity of 250 kN. Specimens of different geometries (cubic and prismatic) were subjected to uniaxial compression at a constant loading rate of 0.05 kN/s. Axial deformation was monitored using a displacement sensor with a travel range of 20 mm. According to ASTM C39M-03, a correction factor of 0.87 was applied to account for the non-standard height-to-diameter ratio of the specimens. The compressive strength, Rc (MPa), was calculated using Equation (6):

$$R_c = \frac{F_{c,max}}{S} \quad (6)$$

where $F_{c,max}$ is the maximum applied load (N) and S is the initial cross-sectional area of the specimen (mm^2).

The overall experimental methodology adopted in this study was designed to ensure the reproducibility, reliability, and multi-scale characterization of the developed bio-based clay composites intended for sustainable construction applications. The experimental procedures and interpretation of the FTIR, XRD, SEM/EDX, and thermogravimetric analyses were established based on previously reported methodologies commonly used for the characterization of sustainable cementitious and aluminosilicate materials [15-23].

For each formulation, mechanical tests were performed on at least three replicate specimens to ensure experimental reproducibility. The reported values correspond to the arithmetic mean ± standard deviation, and error bars representing standard deviations were included in the graphical presentation of the mechanical results to evaluate data variability and measurement consistency.

3. Results and discussion

3.1. Geotechnical and Physicochemical Characterization Parameters

Table 2 highlights significant differences in the geotechnical properties of the Green, Red, and Yellow clayey materials, particularly in terms of plasticity, swelling potential, natural moisture content, and loss on ignition (LOI). These parameters directly influence the suitability of the clayey materials for various environmental and geotechnical applications.

All samples exhibited nearly neutral pH values, ranging from 7.15 to 7.84, which are typical of natural clayey materials and suggest a minimal risk of inducing chemical imbalance in their environment. However, pH alone does not fully determine chemical stability. The Red clayey material showed the highest natural moisture content at 3.06 %. This value may reflect both local environmental conditions, such as recent wetting and drying cycles, and the sample's intrinsic properties, including mineralogical composition and porosity. In contrast, the Green clayey material recorded the highest swelling index at 3.22 %. The presence of phyllosilicate minerals such as illite and kaolinite contributes to the materials' physicochemical behavior. The Yellow clayey material exhibited the lowest swelling index at 1.65 %, indicating improved dimensional stability under humid conditions.

The plasticity index was highest in the Red clayey material (8.6 %), indicating increased sensitivity to moisture variations and greater formability, although this may also be associated with a higher risk of shrinkage. The low plasticity indices observed in all samples support the absence of significant amounts of smectite or other swelling clay minerals, as also confirmed by XRD results. These observations are consistent with the findings of Sørensen et al. [43], who reported a strong relationship between plasticity index, swelling pressure, and workability in fine-grained soils. The Yellow clayey material also displayed the highest liquid limit at 31.35%, reflecting a greater tendency to flow under elevated moisture conditions. The LOI values varied significantly across the samples, with the Yellow clayey material reaching the highest value at 28.22 %. This is likely due to its higher content of organic matter or carbonates, a characteristic particularly relevant for thermal treatments such as sintering or firing. These results align with those reported by Gu et al. [44], who noted that elevated LOI values in natural clayey materials often indicate the presence of thermally unstable components that strongly influence thermal performance.

Table 2. Physicochemical properties of the studied clayey materials

Parameters	pH	W (%)	Swelling Index SI (%)	Plastic limit. PL (%)	Liquid Limit LL	Plasticity Index PI	LOI (%)
Green clayey material	7.84	1.52	3.22	18.55	24.85	6.3	20.12
Red clayey material	7.15	3.06	2.8	17.3	25.9	8.6	26.7
Yellow clayey material	7.57	1.42	1.65	25.15	31.35	6.2	28.22

3.2. Influence of Particle Size and Organic Matter on Plasticity Behavior

The Casagrande plasticity chart (**Figure 5**) illustrates the classification of the studied clayey materials based on their plasticity index (PI) and liquid limit (LL). All three samples fall below the A-line in the Casagrande plasticity chart, suggesting low-plasticity fine-grained soils predominantly exhibiting silt-type characteristics [45]. Among the materials, the Red clayey material (PI = 8.6, LL = 25.9) plots closest to the A-line, reflecting slightly higher clay activity. The Green clayey material (PI = 6.3, LL = 24.85) also falls well below the line, confirming its classification as a low-plasticity fine-grained material. The Yellow clayey material exhibits the highest liquid limit (LL = 31.35), but its plasticity index remains low (PI = 6.2), placing it near the A-line and suggesting silty or low-activity clay behavior. These plasticity trends are strongly consistent with the particle-size distribution of the samples. As shown by the granulometric results, all three

materials contain significant proportions of silt and fine sand, which naturally dilute clay activity and reduce the capacity for water adsorption and interlayer swelling. This explains why PI and LL decrease proportionally with increasing non-clay content, as previously demonstrated for Miocene clayey formations [46]. The Red clayey material, which shows the highest PI, contains the largest proportion of fine clay fraction (< 2 µm), whereas the Yellow clayey material contains more coarse silt, which is consistent with its lower plasticity despite a higher liquid limit. The role of organic matter must also be considered in explaining the observed plasticity behavior. Even though the organic matter content remains relatively low in all samples, its presence tends to reduce interparticle attraction and weaken the clay fabric, leading to lower cohesion and plasticity. This effect is particularly noticeable in the Yellow clayey material sample, where slightly elevated organic content combined with a coarser granulometric profile contributes to its low PI. Such interactions among particle-size distribution, plasticity, and organic matter are central to the objectives of this study, as they influence both the geotechnical behavior of the clayey materials and their suitability for environmental or engineering applications.

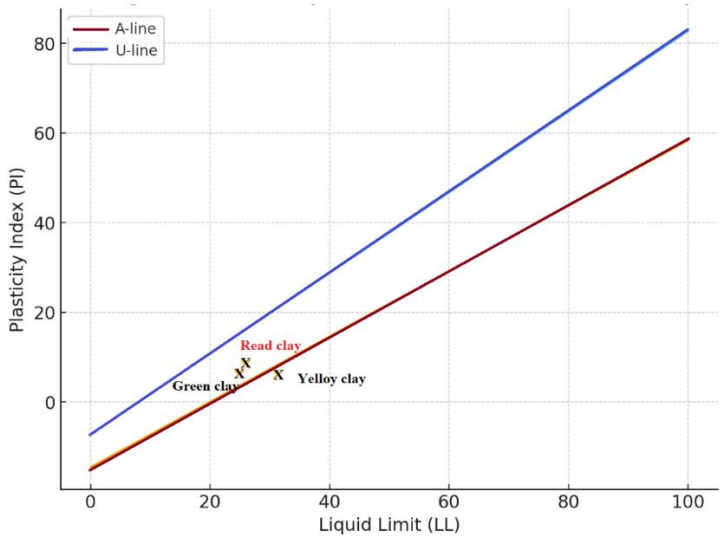

Figure 5. Casagrande plasticity chart of the studied clayey materials

3.3. FTIR Analysis

Figure 6 presents the FTIR spectra of the Red, Green, and Yellow clayey material samples. The FTIR spectra mainly display absorption bands of carbonates and silicates, whereas bands typically assigned to clay minerals, particularly OH groups, are weak or not readily assignable, suggesting that clay-mineral-related OH vibrations are partially masked by dominant carbonate and silicate absorption bands. Although the FTIR spectra display relatively weak hydroxyl-related bands, the XRD quantitative analysis confirms the presence of significant illite and measurable kaolinite contents. This apparent discrepancy may result from FTIR sensitivity limitations, peak overlap effects, and the dominant contribution of carbonate phases. The absorption band observed at 3620 cm^{-1} is attributed to the O-H stretching vibrations of structural hydroxyl groups in phyllosilicates such as kaolinite and illite [47]. In contrast, the broader band near 3417 cm^{-1} is more likely due to the stretching vibrations of adsorbed water or interlayer water molecules rather than structural O-H in clay minerals, as documented in the literature. These bands were more intense in the Green and Yellow samples, indicating higher levels of hydroxylation or water content compared with the Red sample. This observation is consistent with the findings of Zhang et al. [48] and Costa et al. [49], who demonstrated a correlation between O-H absorption intensity and hydration level in natural clayey materials. The absorption peak near 1024 cm^{-1}, present in all three samples, corresponds to Si-O-Si or Si-O-Al stretching vibrations typical of the tetrahedral framework in clay minerals. The bands observed around 870, 784, and 710 cm^{-1} are associated with the

bending vibrations of Al-OH and Si-O bonds, confirming the presence of layered aluminosilicate structures. The Green and Yellow samples exhibited more defined peaks in this region, suggesting greater structural order or higher purity. A band near 1440 cm^{-1}, observed in all samples and characteristic of the asymmetric stretching of carbonate ions (CO_3^{2-}), confirms the presence of calcite or other carbonate phases. However, because FTIR band intensity does not directly reflect quantitative content, the interpretation of carbonate abundance is based primarily on XRD results, which indicate that the Yellow clayey material contains the highest carbonate content. This finding is in line with results reported by Singh et al. [50], who associated similar bands in red clayey material with natural mineral impurities. At lower frequencies, particularly below 600 cm^{-1}, a distinct peak at 534 cm^{-1} was observed. This peak is typically assigned to metal-oxygen (M-O) vibrations, where M may be aluminum, iron, or silicon. These low-frequency bands are essential for identifying the types of metal oxides present in the clay matrix [51]. The peaks observed around 2500 cm^{-1} in the FTIR spectra (**Figure 6**) are characteristic of carbonate groups, confirming the presence of minerals such as calcite and dolomite. This interpretation is consistent with the XRD results (**Figure 7 and Table 2**), which show significant amounts of calcite and dolomite, particularly in the Yellow and Red clayey materials. Thus, the FTIR and XRD analyses are complementary, both indicating a high carbonate content in these samples.

In summary, FTIR analysis confirmed the typical spectral features of clay minerals across all samples, with noticeable differences in hydration levels, structural organization, and carbonate content. These variations reflect the distinct geological origins and mineralogical compositions of the three clayey materials types.

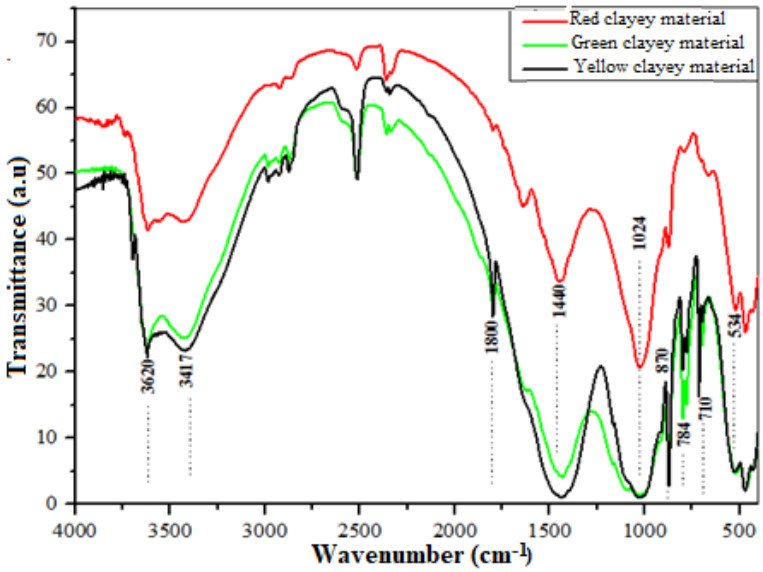

Figure 6. FTIR spectra of the clayey materials samples

3.4. Mineralogical Characterization Using XRD and XRF

The mineralogical and chemical characterization of the clayey materials samples, carried out using X-ray diffraction (XRD) and X-ray fluorescence (XRF), reveals strong consistency between chemical composition and the identified mineral phases, as shown in **Table 3** and **Figure 7**. The XRF results show that the Green clayey material sample has a high SiO2 content (40.43 %), reflecting a significant abundance of quartz, as confirmed by the intense peaks around $2\theta \approx 22°$ and 27° in the XRD diffractograms, in agreement with recent literature [52]. The variation in Al2O3 content, from 6.89 % in the Red clayey material to 15.43 % in the Green clayey material, suggests a variable proportion of aluminosilicate phases such as illite or kaolinite. The presence of illite is indicated by a characteristic peak around 10° (2θ) in **Figure 7** and is confirmed by quantitative XRD analysis [53]. High CaO levels in the Yellow (28.58%) and Red (24.11%) clayey materials correlate with the strong presence of carbonates, mainly calcite and dolomite, identifiable by reflections at 20°, 27°, 34°, 40°, and 45° for calcite and around 33° for dolomite in the XRD patterns [54]. The high MgO content

in the Red clayey material (5.55 %) indicates the presence of mixed carbonate phases, although these are less discernible in the diffractograms. The Fe_2O_3 content, which is highest in the Green clayey material (5.19 %), could explain the presence of minor peaks or elevated backgrounds in the XRD results, attributed to iron oxides or iron-rich clay minerals. The loss on ignition values, particularly high for the Yellow (26.92%) and Red (25.9%) clayey materials, reflect a significant amount of volatile compounds resulting from the decomposition of carbonates and the release of structural water during heating. In contrast, the Green clayey material, with a lower LOI (18.83 %), is consistent with its silicate-dominated composition and lower carbonate content. Altogether, these results confirm that the Green clayey material is primarily composed of silicate minerals (quartz, illite, and kaolinite), while the Yellow and Red clayey materials are characterized by a high proportion of carbonates, mainly calcite and dolomite. This directly influences their properties for use as eco-friendly construction materials. The abundance of silicates in Green clayey material may contribute to improved thermal stability, whereas the presence of carbonates in the other samples may influence their thermal and physicochemical behavior. These observations, in line with recent studies [55,56], highlight the suitability of the different natural clayey materials studied for sustainable construction applications, with each type offering specific advantages depending on its mineralogical and chemical composition.

Table 3. Mineralogical composition (%) of the clayey materials samples

Mineral Phase (%)	Red clayey material	Yellow clayey material	Green clayey material
Calcite	24.78	50.35	38.67
Dolomite	6.43	1.09	0.00
Siderite	0.00	0.02	0.00
Ankerite	1.73	0.34	0.00
Magnesite	1.16	0.05	0.29
Quartz	28.52	12.68	29.38
Pyrite	0.37	0.12	0.20
Illite	24.97	25.42	25.06
Kaolinite	4.76	8.02	3.01
Albite	0.00	0.19	0.93
Anorthite	2.56	0.46	0.12
K-Feldspar	4.71	1.27	2.33
CO_2_XRD	15.33	22.84	17.16

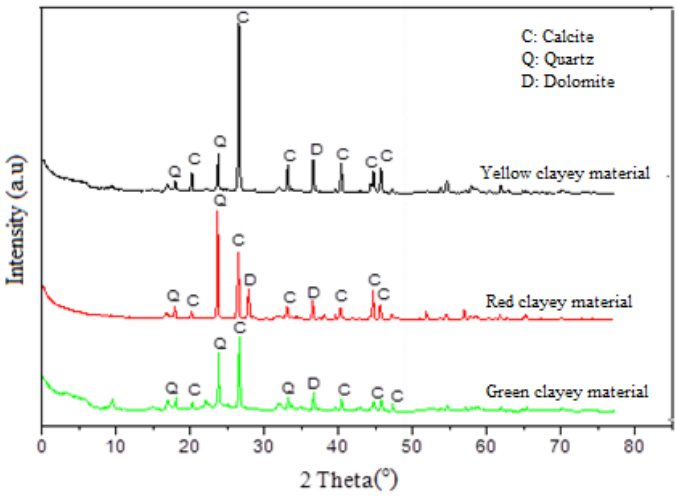

Figure 7. XRD patterns of the clayey materials samples

3.5. Granulometric Characterization

Figure 8 presents the cumulative particle-size distribution of the three clayey materials samples (Red, Green, and Yellow), expressed as passing volume (%) versus particle diameter. Overall, the three materials are dominated by fine fractions, in agreement with the granulometric data. The Green clayey material (38% clay, 52% silt, 10% sand) and Red clayey material (35% clay, 50% silt, 15% sand) exhibit higher proportions of clay and silt, whereas the Yellow clayey material (30% clay, 50% silt, 20% sand) contains a relatively higher sand fraction. The Yellow clayey material shows a more gradual particle-size distribution curve, reflecting the presence of a higher proportion of coarse particles and a wider granulometric spread. In contrast, the Green clayey material exhibits a finer and more homogeneous distribution, as indicated by a steeper curve, while the Green clayey material displays intermediate behavior between the Yellow and Red clayey materials. These granulometric differences are of scientific importance, as particle size directly influences key properties such as specific surface area, porosity, and adsorption capacity. Tripathy and Rao [57] showed, using BET surface area analysis, that reducing the particle size of red clay significantly increases its specific surface area, thereby enhancing both its reactivity and mechanical performance. Similarly, Wang et al. [58] showed that the fine fraction in soils significantly affects pore structure, thereby influencing water retention and adsorption potential. Given its finer and narrower particle-size distribution, the Yellow clayey material may interact more strongly with molecules or ions within a matrix, which can be advantageous for applications such as adsorption or incorporation into composite materials. In contrast, the coarser particle profile of the Red clayey material may result in a different porosity pattern, which can be beneficial for specific geotechnical uses.

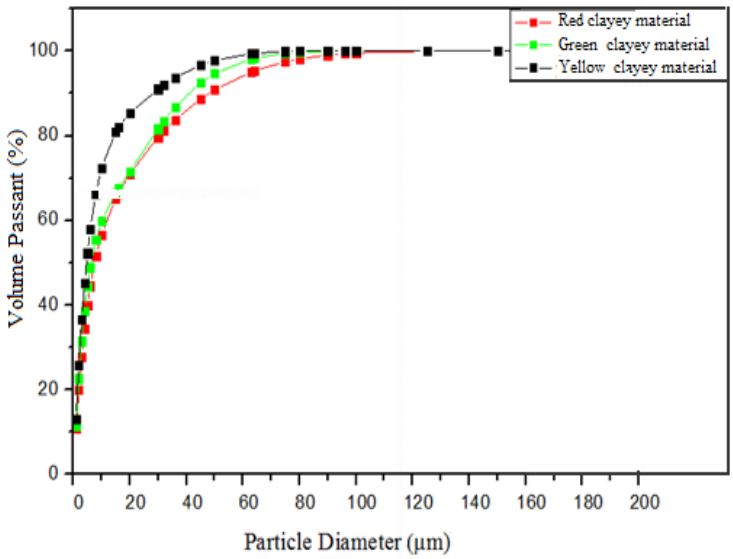

Figure 8. Granulometric distribution curves of Red, Green, and Yellow clayey materials

Additional differential particle-size distribution analysis using dV/dlog(D) curves confirmed the broader granulometric distribution of the yellow clayey material and the finer, narrower distribution of the red clayey material. The green clayey material exhibited an intermediate distribution profile. These results further support the observed differences in plasticity, packing density, and compaction behavior among the studied materials.

3.6. Stratigraphy and Mineral Composition of Red, Yellow, and Green Clayey materials

The stratigraphy and mineral composition of the Red, Yellow, and Green clayey materials sampled at a depth of 40 cm reveal clear lithological and sedimentological contrasts that reflect variable depositional dynamics within the M'sila basin. Granulometric data show that the Green clayey material (38% clay, 52% silt, 10% sand), Red clayey material (35% clay, 50% silt, 15% sand), and Yellow clayey material (30% clay, 50% silt, 20% sand) are dominated by fine fractions, indicating low-energy floodplain and overbank depositional environments consistent with fluvial facies models [59,60]. Mineralogical analysis (XRD) indicates

that illite (~25%) is the principal clay mineral in all samples, accompanied by kaolinite (3-8%) and significant amounts of non-clay minerals such as calcite (24-50%), quartz (12-30%), dolomite, ankerite, magnesite, feldspars (albite, anorthite, and K-feldspar), and minor pyrite. The markedly higher calcite content in the Yellow clay (~50%) suggests enhanced carbonate input or precipitation, whereas the Red and Green clays exhibit more balanced siliceous and carbonate contributions. Such mixed detrital-carbonate assemblages are characteristic of continental semi-arid floodplain deposits and have been documented in recent sedimentological and mineralogical studies of non-marine clay-rich systems [61,62]. Stratigraphically, the vertical profile reveals three sub-horizons:

(i) an upper laminated silty clay (0-15 cm), corresponding to the Fl facies typical of episodic overbank flooding;

(ii) a massive mudstone horizon (15-30 cm), attributed to Fm facies representing suspension settling in stagnant floodplain ponds; and

(iii) a lower silty to sandy clay horizon (30-40 cm) with weak heterolithic structures indicative of intermittent higher-energy inputs and transitional levee or crevasse-splay conditions [59,63]. The granulometric contrast, particularly the higher sand fraction in the Yellow clayey material, correlates well with the lower transitional facies, whereas the more clay-rich Red and Green samples correspond to the massive mid-horizon. The dominance of illite with subordinate kaolinite and feldspars suggests a primarily detrital origin with limited chemical weathering, consistent with semi-arid climatic regimes characterized by episodic sediment supply and weak pedogenic alteration [64].

Overall, the integration of mineralogical, granulometric, and facies evidence provides a coherent interpretation of the spatial and vertical variability of the M'sila clayey materials and highlights their relevance for geotechnical, ceramic, and environmental applications. The particle-size distribution analysis indicates that the Green clayey material has the highest proportion of fine particles (38% clay, 52% silt, 10% sand), followed by the Red clayey material (35% clay, 50% silt, 15% sand), whereas the Yellow clayey material contains more coarse particles (30% clay, 50% silt, 20% sand). As a result, the Green clayey material, with its finer texture and higher content of clay and silt, displays superior plasticity and cohesion, making it particularly suitable for raw earth plasters and applications requiring high workability. The Red clayey material, with a balanced granulometric profile, combines good plasticity with mechanical strength, making it versatile for compressed earth blocks (CEB) and rammed earth construction. In contrast, the Yellow clayey material, with its higher sand content, is better suited for stabilized earth masonry and applications where compaction and dimensional stability are important. Overall, the Green clayey material is considered the most suitable for construction materials requiring excellent workability and cohesion, whereas the Red clayey material appears optimal for general earth construction and the Yellow clayey material is preferable for stabilized earth products.

3.7. Chemical Composition Analysis Using X-ray Fluorescence (XRF)

Although these materials are locally designated as clays, integrated mineralogical and chemical analyses (XRD, FTIR, TGA/DTG, and XRF) indicate that they are predominantly carbonate- and quartz-rich, with only minor amounts of true clay minerals such as illite and kaolinite. XRD patterns exhibit weak or nearly absent reflections for clay minerals (**Figure 7**), whereas FTIR spectra lack distinct OH absorption bands assignable to phyllosilicates (**Figure 6**), both suggesting a low clay mineral content [65,66]. This interpretation is further supported by relatively low Al_2O_3 levels in the XRF data (**Table 4**). These results also indicate that quantitative XRD may overestimate clay mineral fractions due to peak overlap and matrix effects in carbonate-dominated samples [67]. Therefore, the term "clay" is used here in a geotechnical and field-based sense rather than as a strict mineralogical classification. Conversely, high CaO concentrations, 28.58 % in the Yellow sample and 24.11% in the Red sample, are consistent with abundant calcite, as confirmed by XRD, the high LOI values, and the absence of characteristic dehydroxylation weight loss between 400 and 650 °C in the TGA/DTG

profiles. Elevated SiO_2/Al_2O_3 ratios (4.53 for Red, 2.78 for Yellow, and 2.61 for Green) indicate a significant proportion of free silica, particularly in the Red sample [68]. The presence of other oxides (Fe_2O_3, MgO, K_2O, and Na_2O) further supports the occurrence of accessory mineral phases. This mineralogical assemblage directly governs the geotechnical and physicochemical behavior of the materials and must be considered when classifying them and assessing their suitability for applied uses.

Table 4. Chemical composition (%) of clayey materials samples

Components (%)	Red clayey material	Yellow clayey material	Green clayey material
SiO_2	31.278	26.425	40.43
Al_2O_3	6.893	9.487	15.432
Fe_2O_3	3.04	4.666	5.194
CaO	24.113	28.581	13.531
MgO	5.551	1.965	2.388
SO_3	0.622	0.211	0.132
P_2O_5	0.155	0.129	0.111
K_2O	1.629	1.75	2.76
Na_2O	0.064	0.17	0.188
TiO_2	0.386	0.457	0.768
Mn_2O_3	0.04	0.087	0.044
SrO_2	0.056	0.056	0.051
ZnO	0.005	0.007	0.012
Cr_2O_3	0.01	0.011	0.014
LOI	25.9	26.92	18.83

3.8. Influence of Particle Size, Plasticity, and Organic Matter on the Suitability of Clayey materials for Sustainable Construction

The particle-size distribution, plasticity, and organic matter content of the studied clayey materials play a key role in their suitability for eco-friendly construction materials. Finer particles increase plasticity and liquid limit, whereas higher silt or sand contents tend to reduce these properties, resulting in more stable and less deformable clayey materials. The low plasticity observed in our samples is advantageous because it reduces the risk of cracking and shrinkage. In addition, moderate levels of organic matter can enhance workability during shaping, whereas excessive amounts may compromise the final strength of fired products. Together, these factors determine the processing behavior and performance of the clayey materials, directly supporting the objectives of developing sustainable and durable construction materials.

3.9. Thermogravimetric Analysis (TGA)

Thermogravimetric analysis was employed to investigate the thermal transformation pathways and physicochemical reactivity of the natural clayey materials samples. As shown in **Figure 9**, the TGA curves exhibit three major stages of mass loss corresponding to successive dehydration, dehydroxylation, and carbonate decomposition reactions. These thermally induced transformations provide important information regarding the activation behavior and potential pozzolanic reactivity of the studied materials.

The first stage, occurring below approximately 200 °C, is attributed to the evaporation of physically adsorbed water and interlayer moisture weakly bound to the mineral surfaces. The associated weight loss ranged from approximately 2.7 % for the Yellow and Red clayey materials to nearly 5 % for the Green clayey material. This initial dehydration stage reflects the hygroscopic behavior and surface hydration capacity of the materials. The higher moisture retention observed for the Green clayey material may be related to its finer

particle distribution and higher specific surface area rather than to its kaolinite content, since XRD analysis revealed that this sample contains the lowest proportion of kaolinite (3.01 %). From a process-engineering perspective, this low-temperature dehydration stage is important because it governs the preliminary energy demand during thermal activation and drying operations.

The second stage, observed mainly between 450 and 650 °C, corresponds to the dehydroxylation of structural hydroxyl groups associated with phyllosilicate minerals such as kaolinite and illite. This transformation involves the breakdown of hydroxylated aluminosilicate layers and the progressive formation of amorphous reactive phases. The principal reaction associated with kaolinite transformation may be expressed as follows (Equation (7)):

$$Al_2Si_2O_5(OH)_4 \rightarrow Al_2Si_2O_7+2H_2O \quad (7)$$

This reaction leads to the formation of metakaolinite, which is recognized as a highly reactive pozzolanic precursor. The corresponding mass loss reflects the release of chemically bonded hydroxyl groups and therefore provides indirect information regarding the activation potential of the clayey system. Although all samples exhibited thermal events within this temperature range, the intensity and extent of dehydroxylation differed according to mineralogical composition and crystallinity. The Green clayey material displayed less pronounced mass loss in this region, consistent with its lower kaolinite fraction, whereas the Red clayey material exhibited stronger thermal activity, suggesting the presence of more reactive hydroxylated phases or structurally disordered aluminosilicates [69,70].

The third stage, occurring mainly between 700 and 900 °C, is characterized by substantial mass loss associated with the thermal decomposition of carbonate minerals such as calcite and dolomite. These reactions generate gaseous CO_2 and corresponding oxide phases according to the reactions (8) and (9):

$$CaCO_3 \rightarrow CaO + CO_2 \quad (8)$$

$$CaMg(CO_3)_2 \rightarrow CaO+MgO+ 2CO_2 \quad (9)$$

The Yellow and Red clayey materials exhibited the highest mass losses in this region, which correlates well with their elevated CaO contents determined by XRF analysis (28.58 % and 24.11 %, respectively). In contrast, the Green clayey material showed lower carbonate decomposition intensity and improved thermal stability due to its lower carbonate fraction (13.53 %). The decomposition of carbonates is particularly relevant for thermal process optimization because it strongly affects energy consumption, gaseous emissions, and the generation of reactive alkaline oxide phases capable of participating in secondary pozzolanic reactions [71,72].

The total mass loss values (LOI) reached 26.92 % for the Yellow clayey material, 25.90 % for the Red clayey material, and 18.83 % for the Green clayey material. These values reflect the cumulative release of physically adsorbed water, structural hydroxyl groups, carbon dioxide from carbonate decomposition, and traces of volatile impurities. The relatively high LOI values observed for the Yellow and Red clayey materials indicate greater thermal reactivity and more extensive physicochemical transformation during calcination.

Overall, the TGA results demonstrate that the investigated clayey materials behave as reactive mineral systems undergoing successive thermochemical transformations rather than inert geological materials. The combination of dehydration, dehydroxylation, and carbonate decomposition governs the formation of reactive aluminosilicate and alkaline phases, which are critical for potential applications involving thermal activation, adsorption, catalytic supports, or pozzolanic binders. These findings therefore provide a valuable basis for process-oriented optimization of calcination conditions and for evaluating the chemical activation efficiency of these naturally occurring mineral resources.

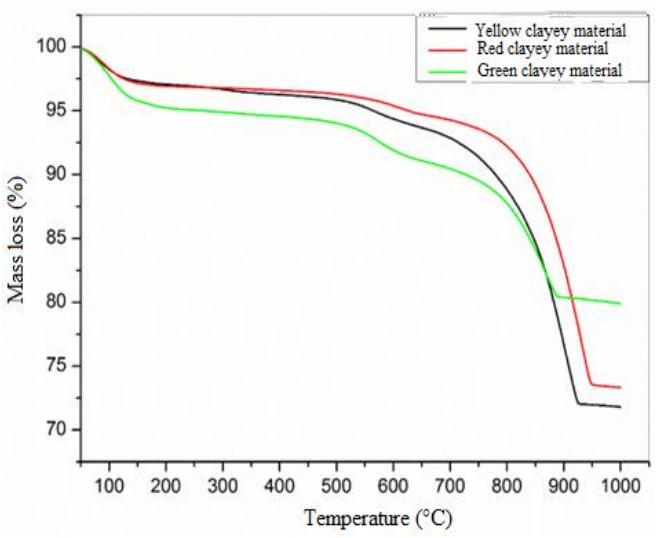

Figure 9. TGA thermograms of the clayey materials samples

3.10. DTG Analysis of Multi-Step Decomposition in Colored Clayey materials

The DTG thermograms of the Red, Green, and Yellow clayey materials reveal a complex multi-step decomposition process occurring between 30 and 1000 °C (**Figure 10**). The derivative thermogravimetric profiles provide additional insight into the kinetics and intensity of the thermal reactions identified in the TGA analysis by clearly distinguishing the temperatures corresponding to maximum decomposition rates.

The first DTG peak detected below 200 °C corresponds to the desorption of physically adsorbed and interlayer water molecules. This endothermic process is characteristic of hydrated aluminosilicate systems and indicates the release of weakly bonded water associated with surface hydration phenomena. The relatively low intensity of this peak suggests that the dehydration process is governed mainly by surface desorption rather than structural transformation. Nevertheless, this stage remains important for thermal process engineering because it influences the initial energy demand during drying and preheating operations [73].

A second and more significant DTG event appears between approximately 400 and 700 °C and corresponds to the dehydroxylation of clay minerals. This process involves the removal of structural hydroxyl groups from phyllosilicate lattices, leading to the collapse of crystalline order and the formation of amorphous aluminosilicate phases with enhanced chemical reactivity. The dehydroxylation reaction is particularly important because it controls the generation of thermally activated pozzolanic phases capable of participating in secondary cementitious reactions. In this temperature range, the Red clayey material exhibits the most pronounced DTG peak, indicating either a higher concentration of hydroxylated mineral phases or a greater degree of structural disorder favoring thermal activation. The broader DTG peaks observed for the Green and Yellow clayey materials suggest a more progressive decomposition mechanism and potentially lower reaction kinetics [74].

The third DTG peak, observed mainly between 850 and 980 °C, is associated with carbonate decomposition reactions involving calcite and dolomite phases. The strong DTG signal observed for the Red clayey material indicates intense decarbonation activity and substantial CO_2 evolution. This thermal event corresponds to the dissociation of carbonate minerals into reactive oxide phases, which may subsequently participate in secondary mineral transformations or alkaline activation reactions. In addition to carbonate decomposition, high-temperature transformations involving iron-bearing phases may also contribute to the observed DTG signal, including structural rearrangements and reduction reactions affecting hematite-containing minerals [75].

The differences in DTG peak intensity, width, and decomposition temperature among the three samples indicate significant variations in thermal reaction pathways and mineral stability. The Green clayey material demonstrates comparatively higher thermal stability, as evidenced by delayed decomposition onset and lower peak intensity. This behavior may be attributed to its higher proportion of stable silicate phases and lower carbonate content. In contrast, the Red and Yellow clayey materials exhibit greater thermal reactivity because of their carbonate-rich composition and more pronounced dehydroxylation behavior. The principal thermochemical transformations identified from the TGA/DTG analyses, together with their corresponding temperature intervals, DTG maximum decomposition temperatures (DTGmax), representative reactions, and estimated mass losses, are summarized in **Table 5**.

Table 5. Thermochemical reaction pathways and characteristic decomposition parameters derived from TGA/DTG analyses

Thermal stage	Temperature range (°C)	DTGmax (°C)	Main transformation	Representative reaction	Estimated mass loss (%)	Theoretical interpretation
Stage I	30–200	95–120	Dehydration and desorption of physically adsorbed water	$H_2O_{ads} \rightarrow H_2O_{gas}$	2.7–5.0	Release of interlayer and surface water
Stage II	450–650	510–540	Dehydroxylation of phyllosilicates	$Al_2Si_2O_5(OH)_4 \rightarrow Al_2Si_2O_7 + 2H_2O$	4–8	Formation of reactive amorphous metakaolinite
Stage III	700–900	850–890	Decarbonation of calcite/dolomite	$CaCO_3 \rightarrow CaO + CO_2CO$	10–18	Generation of reactive alkaline oxides and CO_2 release
Final stage	>900	930–980	Structural reorganization and mineral stabilization	Recrystallization reactions	Minor	Formation of thermally stable phases

The obtained thermochemical parameters confirm the heterogeneous reactivity of the investigated clayey materials and provide useful information for optimizing thermal activation and calcination processes.

From a chemical engineering perspective, these DTG results provide important information regarding the thermal activation efficiency, decomposition kinetics, and process optimization potential of the investigated materials. The identification of characteristic decomposition intervals is particularly useful for determining optimal calcination temperatures aimed at maximizing the formation of reactive amorphous phases while minimizing excessive energy consumption and carbonate-related CO_2 emissions.

Furthermore, the combined XRF, XRD, FTIR, TGA, and DTG analyses demonstrate that these materials cannot be considered purely clay-rich systems. Instead, they should be regarded as heterogeneous aluminosilicate–carbonate mineral systems in which quartz and carbonate phases dominate over the clay fraction. This mineralogical complexity strongly influences their thermochemical behavior, activation mechanisms, and potential applications in sustainable process-engineered construction materials.

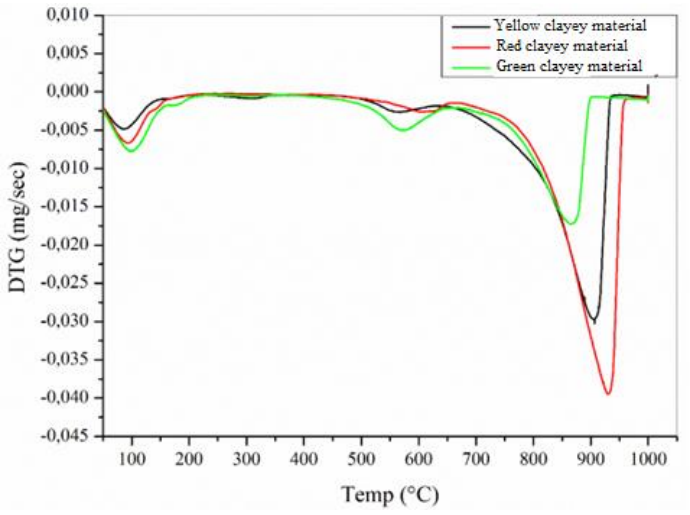

Figure 10. DTG Thermograms of red, green, and yellow clayey materials

3.11. Energy Dispersive X-ray Spectroscopy (EDX) Analysis

The EDX spectra of the Yellow, Red, and Green clayey materials samples (**Figure 11**) reveal the elemental compositions of the materials. All three clays exhibit prominent peaks corresponding to oxygen (O), silicon (Si), and calcium (Ca), which are characteristic of aluminosilicate minerals. Potassium (K) is also present in significant amounts in each sample, indicating the likely presence of feldspar- or mica-type minerals.

The Yellow clayey material shows high concentrations of Ca and Si (**Figure 11a**), consistent with the presence of calcite and quartz phases. The Red clayey material displays a comparable elemental profile, whereas the Green clayey material differs by showing lower calcium intensity and an additional fluorine (F) signal (**Figure 11c**), which may originate from fluorite or related mineral phases. The higher calcium content observed in the Yellow clayey material is consistent with the highest carbonate content identified by XRD and XRF (**Figure 11b**). These variations in elemental composition reinforce the mineralogical distinctions among the three clayey materials. Similar observations were reported by Chihi et al. [76] and Douali et al. [77], who found that clay materials from different geological settings often show variability in their EDX spectra, particularly in the distribution of calcium and potassium.

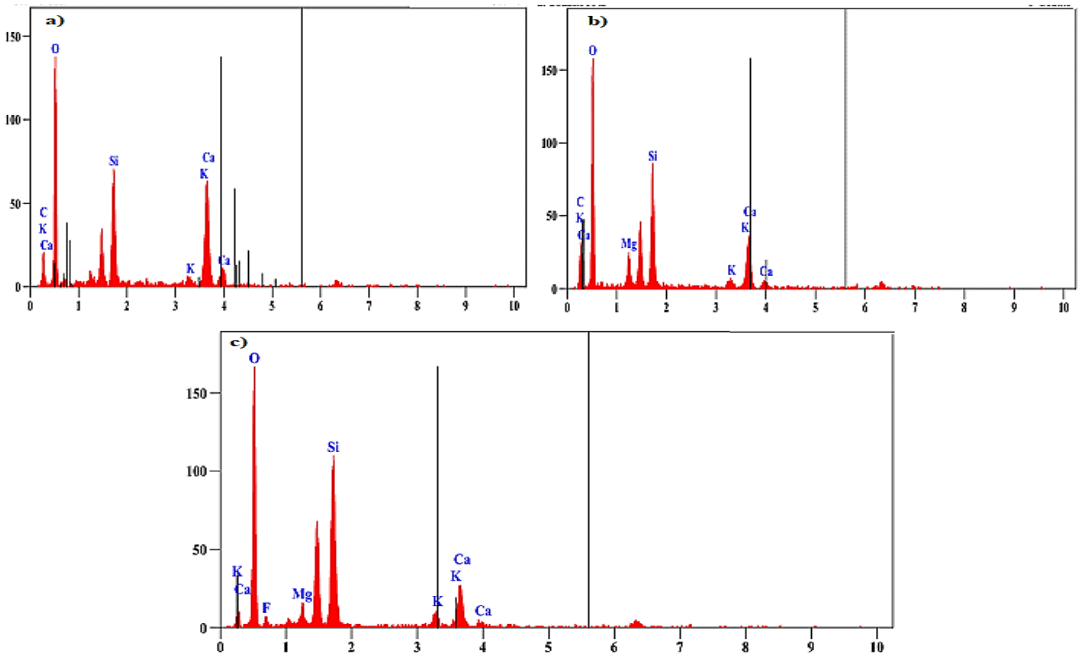

Figure 11. EDX spectra of the clayey materials samples: **(a)** Yellow, **(b)** Red, **(c)** Green

The Ca/Si ratios estimated from the EDX elemental compositions were comparatively higher in the Yellow and Red clayey materials due to their elevated carbonate contents, whereas the Green clayey material exhibited a lower Ca/Si ratio consistent with its silicate-rich composition. This parameter is important because the Ca/Si ratio strongly influences the formation and density of hydration products in stabilized clay systems and may therefore affect the long-term mechanical behavior of the composites.

3.12. Scanning Electron Microscopy (SEM) Analysis

SEM observations (**Figure 12**) reveal clear distinctions in the surface morphologies of the three clayey material samples. The Red clayey material exhibits a compact and dense microstructure composed of closely packed, layered particles. In contrast, the Yellow clayey material presents a more irregular and heterogeneous surface, characterized by rough, disordered agglomerates. The Green clayey material shows a more open structure, with loosely packed, plate-like particles and visible intergranular voids. Although these morphological differences are visually apparent, it is important to note that statements regarding porosity or specific surface area remain qualitative and are not supported by quantitative image analysis such as pore-size distribution or BET measurements. Therefore, any discussion of porosity or surface area should be interpreted with caution. These microstructural features are, however, in line with recent SEM-based studies on natural clayey materials, which emphasize the influence of particle arrangement on thermal behavior and physicochemical properties [78,79]. The technological potential of the studied clayey materials as eco-friendly construction materials is strongly influenced by their mineralogy, organic matter content, particle-size distribution, and plasticity. The predominance of phyllosilicate minerals such as illite, kaolinite, and smectite governs the clays' swelling behavior, thermal stability, and binding capacity. Organic matter, although present in low quantities, can affect thermal degradation and contribute to heterogeneity in mechanical performance. The granulometric distribution, dominated by fine particles (< 50 µm), enhances compaction and cohesion, whereas plasticity parameters reflect the workability required for shaping and forming. Together, these properties provide a comprehensive understanding of the chemical-mineralogical interactions controlling the clayey materials suitability for sustainable construction applications.

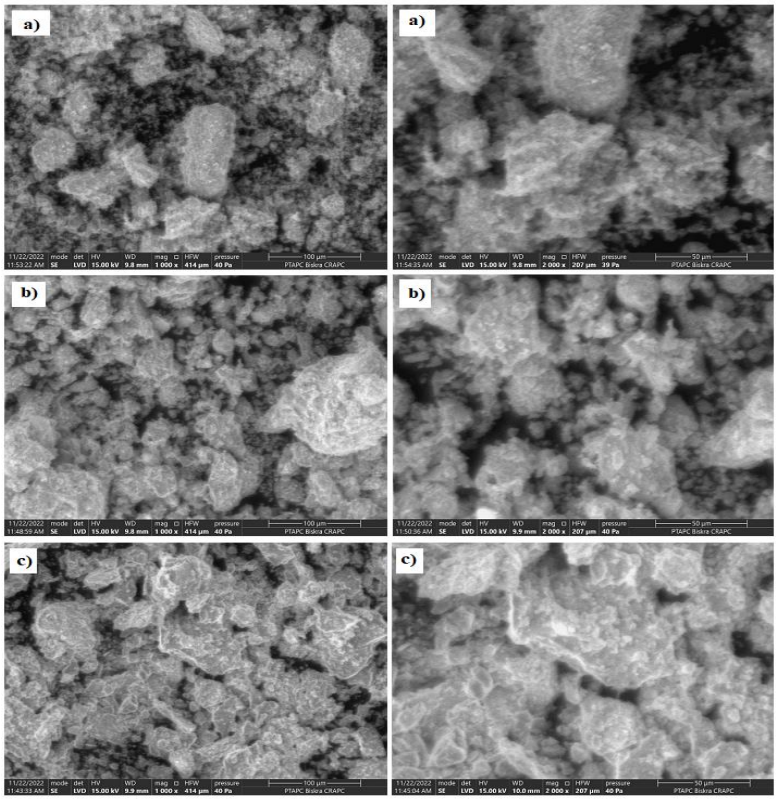

Figure 12. SEM micrographs of the green, red, and yellow clayey materials samples

3.13. Mechanical tests

Figure 13 presents the average compressive and flexural strengths of the investigated clay-based composites together with the corresponding standard deviations obtained from three replicate specimens. Error bars were included to evaluate the reproducibility and statistical variability of the mechanical results.

The incorporation of *Cynodon dactylon* fibers significantly enhances the mechanical properties of the clays, with compressive strength increasing from 2.65 MPa to 3.56 MPa for yellow clay, and flexural strength improving from 0.40 MPa to 0.58 MPa. This improvement is attributed to the fibers' ability to form a binding network that mitigates crack propagation and improves overall cohesion. Such fiber reinforcement aligns well with sustainable material development goals by reducing environmental impact compared to synthetic fibers, as these natural fibers require low energy for production and support biodegradability and circular economy principles. These findings corroborate recent studies where natural fiber reinforcement improved soil mechanical strength by 25 to 40%, while maintaining a low carbon footprint [80]. Similarly, Bui et al. [81] demonstrated that untreated natural fibers effectively enhance the flexural strength of clay soils, contributing to durable mechanical performance. This approach thus offers a viable, eco-friendly solution for construction materials, particularly in regions where these fibers are locally abundant, promoting sustainable resource valorization.

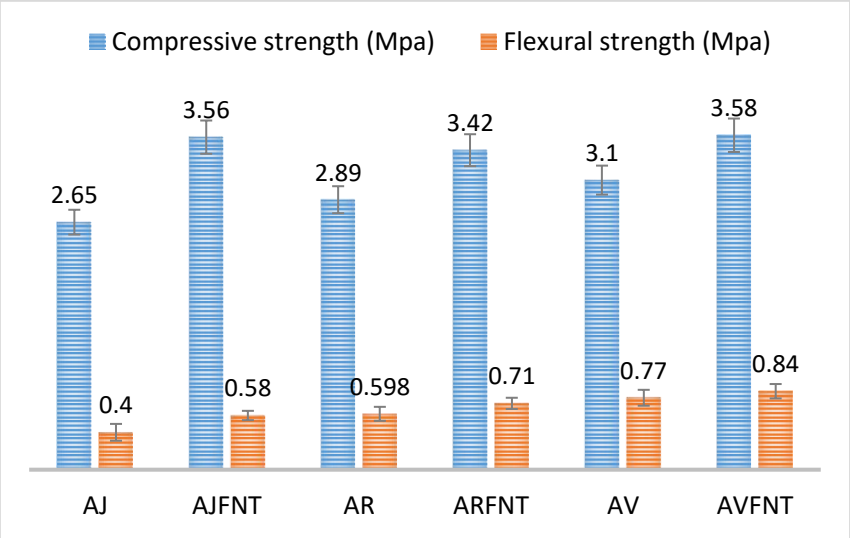

Figure 13. Compressive and flexural strengths of natural clays and composites reinforced with untreated *Cynodon dactylon* fibers

3.14. Comparative Assessment with Other Eco-Friendly Clay-Based Composites

To better evaluate the performance and technological relevance of the developed eco-friendly composites, the obtained mechanical properties were compared with those reported in previous studies involving natural fiber-reinforced earthen or clay-based materials (**Table 6**). The comparison highlights the potential of untreated *Cynodon dactylon* fibers as sustainable reinforcement agents for stabilized clay composites. The developed composites exhibited compressive strengths ranging from 2.65 to 3.56 MPa and flexural strengths between 0.40 and 0.58 MPa, which are comparable to or higher than several previously reported natural fiber-reinforced clay systems. In particular, the incorporation of untreated *Cynodon dactylon* fibers resulted in noticeable improvements in both compressive and flexural behavior, confirming the beneficial role of lignocellulosic fibers in limiting crack propagation and improving stress transfer within the matrix. Compared with synthetic reinforcement systems, the present composites offer several environmental and economic advantages, including low raw-material cost, reduced embodied energy, biodegradability, local availability, and reduced environmental impact. Furthermore, the use of untreated fibers avoids additional chemical processing steps, thereby simplifying fabrication and reducing processing costs. However, some limitations

remain. The mechanical performance of the developed composites is still lower than that of conventional cement-based materials and highly engineered fiber composites. In addition, natural fibers may exhibit variability in composition, moisture sensitivity, and long-term durability under aggressive environmental conditions. Nevertheless, the obtained results demonstrate that the developed materials are promising candidates for sustainable non-structural and semi-structural construction applications, particularly in low-carbon and resource-efficient building systems.

Table 6. Comparison of the developed eco-friendly clay composites with previously reported natural fiber-reinforced earthen materials

Study	Matrix type	Reinforcement	Compressive strength (MPa)	Flexural strength (MPa)	Main advantages	Main limitations
Present study	Stabilized clay	Untreated *Cynodon dactylon* fibers	2.65–3.56	0.40–0.58	Low-cost, biodegradable, locally available, improved crack resistance	Moderate mechanical strength, moisture sensitivity
Bui et al. [82]	Clay soil	Natural plant fibers	2.1–3.0	0.35–0.50	Improved ductility and toughness	Fiber dispersion difficulties
Santos et al. [83]	Earthen blocks	Sisal fibers	1.8–2.9	0.30–0.46	Renewable reinforcement, low density	Reduced durability in humid conditions
Millogo et al. [84]	Adobe material	Straw fibers	1.5–2.5	0.20–0.40	Excellent thermal insulation	Lower compressive resistance
Tang et al. [85]	Cement-stabilized clay	Hemp fibers	3.2–4.5	0.45–0.70	Enhanced mechanical stability	Higher processing cost
Ali et al. [86]	Lime-clay composite	Coconut fibers	2.4–3.1	0.38–0.55	Sustainable and lightweight	Long-term durability concerns

4. Conclusion

The present study provided a comprehensive physicochemical, mineralogical, granulometric, microstructural, and thermochemical characterization of three natural clayey materials collected from the M'sila region (Algeria) and assessed their suitability for sustainable construction applications. Combined XRF, XRD, FTIR, SEM/EDX, TGA, and DTG analyses demonstrated that these materials correspond to heterogeneous aluminosilicate–carbonate systems whose mineralogical composition strongly influences their thermal behavior, physicochemical reactivity, and engineering performance.

The investigated materials exhibited significant differences in mineralogical composition, particle-size distribution, and thermal stability. The Green clayey material, characterized by a higher silicate fraction and lower carbonate content, showed comparatively greater thermal stability and finer granulometric characteristics. In contrast, the Red and Yellow clayey materials displayed stronger carbonate-related thermochemical reactivity, particularly during high-temperature decomposition processes. Microstructural and granulometric analyses further revealed variations in particle organization and texture, which are expected to influence compaction behavior, porosity, and thermal activation efficiency.

Thermogravimetric analyses identified three principal thermal transformation stages associated with dehydration, dehydroxylation, and carbonate decomposition. The dehydroxylation stage between 450 and 650 °C was associated with the formation of reactive amorphous aluminosilicate phases, whereas carbonate decomposition between 700 and 900 °C generated reactive alkaline oxides accompanied by CO_2 release. These

findings provide valuable information for optimizing calcination conditions and improving the efficiency of thermal activation processes.

Mechanical investigations demonstrated that reinforcement with untreated Cynodon dactylon fibres significantly improved the compressive and flexural behavior of the clay-based composites. The incorporation of natural fibres enhanced matrix cohesion and limited crack propagation, confirming the potential of locally available lignocellulosic resources for the development of eco-friendly and low-carbon construction materials.

Overall, the investigated clayey materials exhibited promising potential for sustainable construction applications, particularly for stabilized earth composites and thermally activated mineral systems. Compared with previously reported eco-friendly earthen composites, the developed materials showed competitive mechanical performance while maintaining simplified processing conditions and reduced environmental impact through the use of abundant local resources. Future work should focus on durability assessment, thermal conductivity evaluation, optimization of thermal activation conditions, and life cycle assessment (LCA) in order to further validate the environmental and industrial applicability of these materials.

Author contributions

Conceptualization, Deghfel Nadir and Benyahia Azzedine; methodology, Melouki Azzedine; software, Larkat Karima; validation, Laib Nouri, Melouki Azzedine and Benyahia Azzedine; formal analysis, Larkat Karima; investigation, Laib Nouri; resources, Laib Nouri; data curation, Benyahia Azzedine; writing—original draft preparation, Deghfel Nadir; writing-review and editing, Benyahia Azzedine; visualization, Melouki Azzedine and Laib Nouri; supervision, Deghfel Nadir and Benyahia Azzedine. All authors have read and agreed to the published version of the manuscript.

Acknowledgments

We would like to express our sincere gratitude to Mr. Safer Tabi Ramdan, Director of the “BATEAUX CASSE-M’Sila, Algeria” factory.

We also extend our thanks to Gabriela Kouahla for her valuable proofreading assistance.

Conflict of interest

The authors declare no conflict of interest.

References

1. Benmansour, N., Agoudjil, B., Gherabli, A., Kareche, A., & Boudenne, A. (2014). Thermal and mechanical performance of natural mortar reinforced with date palm fibers for use as insulating materials in building. *Energy and Buildings*, 81, 98–104. https://doi.org/10.1016/j.enbuild.2014.05.034
2. Laborel-Préneron, A., Aubert, J. E., Magniont, C., Tribout, C., & Bertron, A. (2016). Plant aggregates and fibers in earth construction materials: A review. *Construction and Building Materials*, 111, 719–734. https://doi.org/10.1016/j.conbuildmat.2016.02.119
3. Liuzzi, S., Rubino, C., Stefanizzi, P., Petrella, A., Boghetich, G., Casavola, C., & Pappalettere, C. (2018). Hygrothermal properties of clayey plasters with olive fibers. *Construction and Building materials*, 158, 24–32. https://doi.org/10.1016/j.conbuildmat.2017.10.013
4. Minke, G. (2012). Building with Earth (3rd ed.). Birkhäuser. Retrieved from https://www.perlego.com/book/2884768/building-with-earth-design-and-technology-of-a-sustainable-architecture-pdf (Original work published 2012)
5. Heathcote, K. A., & Lawrence, M. (1995). Durability of earth wall buildings. *Construction and Building Materials*, 9(3), 185–189. https://doi.org/10.1016/0950-0618(95)00035-E
6. Houben, H., & Guillaud, H. (1994). *Earth construction: A comprehensive guide*. **Publisher:** Intermediate Technology
7. Ciancio, D., Beckett, C. T. S., & Carraro, J. A. H. (2014). Optimum lime content identification for lime-stabilised rammed earth. *Construction and Building Materials*, 53, 59–65. https://doi.org/10.1016/j.conbuildmat.2013.11.077

8. Millogo, Y., Morel, J.-C., Aubert, J.-E., & Ghavami, K. (2014). Experimental analysis of Pressed Adobe Blocks reinforced with Hibiscus cannabinus fibers. Construction and Building Materials, 52, 71-78. February 2014. DOI: 10.1016/j.conbuildmat.2013.10.094
9. Saidi, M., Cherif, A. S., Zeghmati, B., & Sediki, E. (2018). Stabilization effects on the thermal conductivity and sorption behavior of earth bricks. *Construction and Building Materials*, 167, 566–577. https://doi.org/10.1016/j.conbuildmat.2018.02.063
10. Ashour, T., Korjenic, A., Korjenic, S., & Wu, W. (2015). Thermal conductivity of unfired earth bricks reinforced by agricultural wastes with cement and gypsum. *Energy and Buildings*, 104, 139–146. https://doi.org/ 10.1016/j.enbuild.2015.07.016
11. Naseem, A., Ansari, W. S., Kashif, M., Naseem, A., Sadiq, S., Schotte, K., & De Backer, H. (2023). Comparison of different combined multiple tunnel complexes in soft soil under seismic vibrations. *Civil Engineering Journal*, 9(12), 2958–2969. https://doi.org/10.28991/CEJ-2023-09-12-01
12. Naseem, A., Ansari, W. S., Kashif, M., Sadiq, S., Schotte, K., & De Backer, H. (2023). Evaluating the performance of the twin tunnel complex in soft soil subjected to horizontal ground shaking. *Frontiers in Environmental Science*, 11, 1242296. https://doi.org/10.3389/fenvs.2023.1242296
13. Naghizadeh-Ardebili P, Jozanikohan G, Moradzadeh A. The characterization of clay minerals in the Kashafrud Formation in a gas field in northeast Iran. *Scientific Reports* 2025;15:9000. doi:10.1038/s41598-025-93930-5.
14. Wang, Y., Liu, J., Zhang, P., & Wang, D. (2022). Microstructural and mechanical assessment of sulfate-resisting cement concrete over Portland cement incorporating sea water and sea sand. *Construction and Building Materials*, 335, 127518. https://doi.org/10.1016/j.conbuildmat.2022.127518
15. Zhang, H., Li, Y., & Zhao, X. (2021). Microstructural analysis of corrosion products of steel rebar in coral aggregate seawater concrete. *Materials Characterization*, 176, 111111. https://doi.org/10.1016/j.matchar.2021.111111
16. Khan, M., Ahmad, S., & Amin, M. N. (2022). An experimental study on non-destructive evaluation of the mechanical characteristics of a sustainable concrete incorporating industrial waste. *Journal of Building Engineering*, 46, 103810. https://doi.org/10.1016/j.jobe.2021.103810
17. Li, X., Chen, B., & Wang, Q. (2023). A novel approach to improve carbonation resistance of calcium sulfoaluminate cement by assimilating fine cement-sand mix. *Cement and Concrete Composites*, 137, 104947. https://doi.org/10.1016/j.cemconcomp.2022.104947
18. Zhou, Y., Liu, S., & Chen, H. (2022). Mechanism of blended steel slag mortar with CO_2 curing exposed to sulfate attack. *Journal of Cleaner Production*, 365, 132819. https://doi.org/10.1016/j.jclepro.2022.132819
19. Sun, W., Zhao, Y., & Gao, X. (2021). Analysis of fine sulfoaluminate cement by strength and thermogravimetric analysis. *Thermochimica Acta*, 703, 178998. https://doi.org/10.1016/j.tca.2021.178998
20. Liu, J., Wang, T., & Zhang, Y. (2020). The effects of carbonation and hydration on the mineralogy and microstructure of basic oxygen furnace slag products. *Construction and Building Materials*, 259, 119789. https://doi.org/10.1016/j.conbuildmat.2020.119789
21. Huang, Z., Li, F., & Chen, P. (2021). Influence of fine cement sand paste in preparation of cementitious materials. *Materials*, 14(18), 5342. https://doi.org/10.3390/ma14185342
22. Zhang, L., Wang, H., & Liu, Y. (2021). Effect of bentonite on the sulfate durability of seawater coral-aggregate concrete. *Materials*, 14(9), 2465. https://doi.org/10.3390/ma14092465
23. Meukam, P., Jannot, Y., Noumowe, A., & Kofane, T. C. (2004). Thermo physical characteristics of economical building materials. *Construction and Building Materials*, 18(6), 437–443. https://doi.org/10.1016/j.conbuildmat.2004.03.010
24. Cagnon, H., Aubert, J. E., Coutand, M., & Magniont, C. (2014). Hygrothermal properties of earth bricks. *Energy and Buildings*, 80, 208–217. https://doi.org/10.1016/j.enbuild.2014.05.024
25. Villar, M. V., Martín, P. L., & Barcala, J. M. (2005). Modification of physical and mechanical properties of bentonite by acid treatment. *Applied Clay Science*, 28(1–4), 199–214. https://doi.org/10.1016/j.clay.2004.01.003
26. Kouadri Z. Étude de l'effet du temps de traitement alcalin de fibres palmier sur le comportement mécanique des matériaux à base d'argile rouge de la région de M'sila. *Matériaux & Techniques* 2019;107:404. doi:10.1051/mattech/2019031.
27. Elhamdounia Y, Khabbazia A, Benayada C, Dadib A, Ahmid OI. Effect of fiber alfa on thermophysical characteristics of a material based on clay. *Energy Procedia* 2015;74:718–727. doi:10.1016/j.egypro.2015.07.807.
28. Deghfel N, Benyahia A, Hamrouni A, Rahmouni ZEA, Nouioua K, Belaâda H, et al. Mâadid clay in the M'sila region, Algeria: evaluation and characterization. *Natural Volatiles & Essential Oils* 2022;9(1):1593–1607.
29. Mouissa F, Benyahia A, Djehiche M, Belmokre K, Deghfel N, Redjem A, et al. The effect of chemical treatment on the mechanical and thermal properties of composite materials based on clay reinforced with sawdust. *Matériaux & Techniques* 2021;109:101. doi:10.1051/mattech/2021013.
30. Fung, W. W. S., Kwan, A. K. H., & Wong, H. C. (2018). Mechanical strength and drying shrinkage behavior of earthen construction materials prepared from different soils. *Materials and Structures*, 51(3), 77. https://doi.org/10.1617/s11527-018-1202-1
31. Sayam S. Natural fibers in sustainable materials: Extraction technologies, fiber modification, and performance–sustainability relationships. *RSC Advances* 2026;16:10495–10537. doi:10.1039/D5RA09029F.

32. ASTM International. *Standard test method for particle-size analysis of soils (ASTM D422-63)*. ASTM International; 2007. Available online: https://www.astm.org/d0422-63r07.html (accessed on 08 May 2026).
33. International Organization for Standardization. *ISO 11277:2009. Soil quality — Determination of particle size distribution in mineral soil material — Method by sieving and sedimentation*. ISO; 2009.
34. Bain DC, Smith BJ. *Soil mineralogy with environmental applications*. Cambridge University Press; 2019.
35. Digging into Canadian Soils: An Introduction to Soil Science.," Canadian Journal of Soil Science 102(2), 577-578, (14 March 2022). https://doi.org/10.1139/CJSS-2021-0164
36. Scott, I. S. P. C., Nouwakpo, K., Bjorneberg, D., Rogers, C., & Vitko, L. (2024). Establishing a standard protocol for soil texture analysis using the laser diffraction technique. Soil Science Society of America Journal, 88, 1691–1708. https://doi.org/10.1002/saj2.20738
37. Peng, X., Horn, R., Zhang, B., Zhao, Y., & Wang, L. (2017). Evaluation of the particle sizes of four clay minerals. *Applied Clay Science*, 135, 313–324. DOI: 10.1016/j.clay.2016.10.012
38. Bouhadad Y, Djellit H, Maouche S. Soil horizons and mineral composition in northeast Algeria. *Journal of African Earth Sciences* 2012;66–67:1–15. doi:10.1016/j.jafrearsci.2012.01.002.
39. Velde B. *Introduction to clay minerals: Chemistry, origins, uses and environmental significance*. Chapman & Hall; 1992.
40. Bouaziz R. *L'analyse thermique : les changements de phase*. Gauthier-Villars; 1972.
41. Konan KL, Soro J, Andji JYY, Oyetola S, Kra G. Étude comparative de la déshydroxylation/amorphisation dans deux kaolins de cristallinité différente. 2010;29–39.
42. De Clerck P. *Limites d'Atterberg*. Centre de Recherches Routières, Rapport CR No.14; 1981.
43. Sørensen KK, Okkels N. Correlation between drained shear strength and plasticity index of undisturbed overconsolidated clays. In: *Proceedings of the 18th International Conference on Soil Mechanics and Geotechnical Engineering*; 2–6 September 2013; Paris, France. Presses des Ponts; 2013. Vol. 1, pp. 423–428.
44. Almajed A, et al. Thermal analysis and compositional effects in natural clay ceramics. *Journal of Materials in Civil Engineering* 2024.
45. Moreno-Maroto JM, Alonso-Azcárate J. A new definition of "clay" based on plasticity and its impact on soil classification systems. *Applied Clay Science* 2018;161:57–68.
46. AlHonati Q, Szendefy J, Vásárhelyi B. Effect of changing sand content on liquid limit and plasticity index of clay. *Geotechnics* 2025;5(1):4.
47. Farmer VC. Infrared spectroscopy in clay mineral studies. *Clay Minerals* 1968;7(4):373–387. doi:10.1180/claymin.1968.007.4.01.
48. Zhang Y, Liu M, Yang X. Infrared spectroscopy study on structural hydroxyl groups in clay minerals. *Applied Clay Science* 2021;200:105893. doi:10.1016/j.clay.2021.105893.
49. Costa JA, Oliveira AA, Ferreira C. Spectroscopic insights into the thermal and structural behavior of natural clays. *Spectrochimica Acta Part A: Molecular and Biomolecular Spectroscopy* 2023;294:122566. doi:10.1016/j.saa.2022.122566.
50. Singh R, Sharma M, Tripathi P. Characterization of red clay from various regions of India for potential ceramic applications. *Materials Today: Proceedings* 2022;62:3397–3402. doi:10.1016/j.matpr.2022.03.024.
51. González JM, Barrera EO, Castillo MC. FTIR and XRD characterization of montmorillonite and kaolinite from natural deposits. *Journal of Materials Research and Technology* 2021;12:2450–2459. doi:10.1016/j.jmrt.2021.03.045.
52. Bastida J, Pardo-Ibañez P. Applications of X-ray powder diffraction microstructural analysis in applied clay mineralogy. *Minerals* 2024;14(6):584. doi:10.3390/min14060584.
53. Akinbodunse SJ, Ufer K, Dohrmann R, Mikutta C. Evaluation of the Rietveld method for determining content and chemical composition of inorganic X-ray amorphous materials in soils. *American Mineralogist* 2024;109(12):2037–2051. doi:10.2138/am-2023-9240.
54. Ehrmann W, Wilson PA, Arz HW, Schulz H, Schmiedl G. Clay mineralogy, grain size, XRF geochemistry and Nd and Sr isotopes from the central Red Sea. *PANGAEA* 2023. doi:10.1594/PANGAEA.960352.
55. Ning D, Ma Q, Ge W, Shao Z, Lei T, Xing H. Investigation of the microscopic properties of natural structured clay. *Frontiers in Earth Science* 2023;11:1312326. doi:10.3389/feart.2023.1312326.
56. Shokanov A, Manakova I, Vereshchak M, Migunova A. Characterization of Kazakhstan's clays by Mössbauer spectroscopy and X-ray diffraction. *Minerals* 2024;14(7):713. doi:10.3390/min14070713.
57. Tripathy S, Rao KS. Effect of soil structure and mineralogy on the swelling behavior of Red Clays. *Engineering Geology* 2002;64:273–285.
58. Wang X, Li H, Zhao Y, Chen J. Influence of clay fines on pore structure and water retention in soil systems. *Applied Sciences* 2023;13(4):1887. doi:10.3390/app13041887.
59. Miall AD. *The geology of fluvial deposits: Sedimentary facies, basin analysis, and petroleum geology*. 2nd ed. Springer; 2016.
60. Walker RG. Facies models revisited: From rigid frameworks to fluid systems. *Sedimentary Geology* 2006;202(3):293–299.
61. Bahloul A, Saadi N, Benrabah B. Mineralogical and geochemical characterization of clay-rich floodplain deposits in semi-arid continental basins. *Applied Clay Science* 2021;214:106284.

62. Chen Y, Li X, Wang Q. Clay mineral assemblages and depositional conditions in continental alluvial-floodplain systems. *Journal of Sedimentary Research* 2022;92(4):345–360.
63. Gibling MR, Benyon C. Fluvial facies models revisited: Floodplain processes and sedimentary structures. *Sedimentology* 2020;67(3):1234–1260.
64. Zidan A, El-Sheikh H, Abdallah M. Weathering intensity and clay mineral formation in semi-arid floodplains: Implications for sediment provenance and environmental conditions. *Catena* 2023;228:107090.
65. Mahmoud ZH, Al-Bayati RA, Khadom AA. Electron transport in dye-sensitized solar cell with tin-doped titanium dioxide as photoanode materials. *Journal of Materials Science: Materials in Electronics* 2022;33:5009–5023. doi:10.1007/s10854-021-07690-9.
66. Carretero MI. Clay minerals and their beneficial effects upon human health. *Applied Clay Science* 2002;21(1–2):155–163.
67. Holtz WG, Gibbs HJ. Engineering properties of expansive clays. *Transactions of the ASCE* 1956;121:641–663.
68. Sadki H, Ziat K, Saidi M. Characterization of natural clay materials for engineering applications. *Journal of Materials and Environmental Sciences* 2014;5(S1):2061–2068.
69. Abdelli F, Morsli A, Belattar N. Correlating mineralogical transformations with thermal behavior of Algerian clays. *Clay Minerals* 2022;57:45–58. doi:10.1180/claymin.2022.013.
70. Wang H, Zhou L, Xu G. Coupled TGA-XRD study on clay dehydroxylation and structural transitions. *Applied Clay Science* 2023;228:106801. doi:10.1016/j.clay.2023.106801.
71. Rahmani A, Touati F, Djabri A. Thermal and chemical evaluation of North African dolomitic clays. *Ceramics International* 2022;48(12):17289–17298. doi:10.1016/j.ceramint.2022.03.047.
72. Kacem I, Boukef N, Essafi W. Comparative study of thermal decomposition of natural clays from the Maghreb region. *Journal of African Earth Sciences* 2024;211:104968. doi:10.1016/j.jafrearsci.2024.104968.
73. Zhao Z, Zhang Y, Li B, Xu Y. Thermal behavior and structural changes of natural clays: A thermogravimetric study. *Applied Clay Science* 2020;185:105416. doi:10.1016/j.clay.2020.105416.
74. Chen S, Liu L, Huang J, et al. Investigation of dehydroxylation behavior of kaolinite by thermogravimetry and FTIR. *Journal of Thermal Analysis and Calorimetry* 2021;146:2541–2549. doi:10.1007/s10973-020-10249-0.
75. Kumar A, Singh N, Sahoo SC. Characterization and thermal transformation of clays for ceramic applications. *Ceramics International* 2022;48(3):3746–3754. doi:10.1016/j.ceramint.2021.10.168.
76. Chihi M, Zermane H, Gacem A. Characterization and valorization of natural Algerian clays for ceramic applications. *Applied Clay Science* 2023;236:106759.
77. Douali R, Djellali M, Benabdelkader A. Comparative study of physicochemical properties of red, green, and yellow clays for pharmaceutical use. *Materials Chemistry and Physics* 2022;288:126450.
78. Smith JA, Brown RT, Lee Y. SEM characterization of natural clays: Microstructure and thermal performance. *Applied Clay Science* 2018;155:125–134.
79. Li W, Zhang H. Influence of microstructure on the physicochemical properties of clays: A SEM study. *Clay Minerals* 2020;55(2):145–154.
80. Mohajerani, A., Karunanithi, A.T., Ranjbar, N., Razzaghi-Kashani, M., Nazarian, S., 2020. Mechanical behavior of fiber-reinforced clay soils: A review. *Construction and Building Materials*, 243, 118216. https://doi.org/10.1016/j.conbuildmat.2020.118216.
81. Bui, H.H., Nguyen, T.T., Mai, H.D., Pham, T.M., 2021. Effect of natural fiber reinforcement on the strength characteristics of clayey soils. *Applied Clay Science*, 199, 105849. https://doi.org/10.1016/j.clay.2020.105849.
82. Bui, Q. B., Morel, J. C., Hans, S., & Walker, P. (2009). Effect of natural fibres on the mechanical properties of earth blocks. *Construction and Building Materials*, 23(10), 3241–3247. https://doi.org/10.1016/j.conbuildmat.2009.06.006
83. Santos, S. F., Tonoli, G. H. D., Mejia, J. E. B., Fiorelli, J., & Savastano Jr, H. (2015). Non-conventional cement-based composites reinforced with vegetable fibers: A review of strategies to improve durability. *Materials*, 8(3), 1213–1233. https://doi.org/10.3390/ma8031213
84. Millogo, Y., Morel, J. C., Aubert, J. E., & Ghavami, K. (2014). Experimental analysis of pressed adobe blocks reinforced with Hibiscus cannabinus fibers. *Construction and Building Materials*, 52, 71–78. https://doi.org/10.1016/j.conbuildmat.2013.10.094
85. Tang, C., Shi, B., Gao, W., Chen, F., & Cai, Y. (2007). Strength and mechanical behavior of short polypropylene fiber reinforced and cement stabilized clayey soil. Geotextiles and Geomembranes, 25(3), 194–202. https://doi.org/10.1016/j.geotexmem.2006.11.002
86. Ali, M., Liu, A., Sou, H., & Chouw, N. (2012). Mechanical and dynamic properties of coconut fibre reinforced concrete. *Construction and Building Materials*, 30, 814–825. https://doi.org/10.1016/j.conbuildmat.2011.12.068